$^{10}B(p,n)^{10}C$ reaction at 186 MeV

L. Wang, X. Yang, and J. Rapaport
Ohio University, Athens, Ohio 45701

C. D. Goodman, C. C. Foster, and Y. Wang
Indiana University Cyclotron Facility, Indiana University, Bloomington, Indiana 47405

R. A. Lindgren
University of Virginia, Charlottesville, Virginia 22901

E. Sugarbaker, D. Marchlenski, S. de Lucia, and B. Luther
Ohio State University, Columbus, Ohio 43210

L. Rybarcyk and T. N. Taddeucci
Los Alamos National Laboratory, Los Alamos, New Mexico 87545

B. K. Park
New Mexico State University, Las Cruces, New Mexico 88003
(Received 29 October 1992)

The $^{10}B(p,n)^{10}C$ reaction was studied using the Indiana University Cyclotron Facility (IUCF) neutron time-of-flight facilities at an incident proton energy of 186 MeV between $\theta_{lab} = 0°$ and $\theta_{lab} = 50°$ in steps of 5°. The IUCF neutron polarimeter was also used to measure polarization observables at $\theta_{lab} = 0°$, 15°, and 20° using an incident transverse polarized proton beam. Data for transitions to excited states in ^{10}C below 7 MeV are presented. A multipole decomposition analysis is presented for unresolved states up into the continuum. Distorted wave calculations are presented for positive and negative parity transitions which are compared with data to assess spectroscopies of the ^{10}C excited states.
PACS numbers: 25.40.Ep, 27.20.+n, 24.70.+s

I. INTRODUCTION

The nucleus ^{10}B is probably the only stable nucleus in nature for which, to a good approximation, the dominant component of the ground-state wave function can be described as a stretched configuration, i.e., with two nucleons in the $1p_{3/2}$ subshells coupled to a total angular momentum $J^\pi = 3^+$. Thus, scattering and nuclear reactions on ^{10}B provide a unique case to study transitions between an initial nonspherical target with a very well-described wave function and final states that are more spherical such as the $J^\pi = 0^+$, $T = 1$ isobaric triplet of mass $A = 10$. For this reason and the fact that the low-lying levels are well separated, scattering from ^{10}B has been studied with many probes. In particular, the pure $M3$ electroexcitation of the $T = 0$ ground state of ^{10}B to the $T = 1$, $J^\pi = 0^+$ level at 1.74 MeV in ^{10}B has been studied by Hicks *et al.* [1]. Their results for the $M3$ transition indicate excellent agreement with calculations that employ the *sp* shell single particle wave functions of Cohen and Kurath [2].

Proton scattering from ^{10}B has been studied recently by Lewis *et al.* [3] and by Baghaei *et al.* [4] at 200 MeV. Differential cross section data for the six low-lying levels below 6 MeV excitation energy in ^{10}B are presented in Ref. [3], while differential cross section, analyzing power, induced polarization, and normal polarization transfer coefficient data for the transition between the $^{10}B(3^+$, g.s.) and the $^{10}B(0^+$, 1.74 MeV) state are presented in Ref. [4].

The charge-exchange reaction $^{10}B(^3He,t)^{10}C$ has been studied at $E(^3He) = 30$ and 40 MeV by Mangelson *et al.* [5] and by Schneider *et al.* [6] at $E(^3He) = 38.2$ MeV. In addition to the ground state and first excited state at 3.36 MeV, these authors report level structures centered at $E_x = 5.28$ and 6.58 MeV. Willis *et al.* [7] report on the same reaction but at $E(^3He) = 217$ MeV. They present angular distributions for transitions to the 0^+(g.s.), 2^+(3.36 MeV), and 2^+(5.6 MeV) states in ^{10}C.

The $^{12}C(p,t)^{10}C$ reaction has been reported at intermediate proton energies by Bachelier *et al.* [8] and by Shepard *et al.* [9]. Besides the transitions to the 0^+(g.s.) and to the 2^+(3.36 MeV), these authors report excitations to triton groups at 5.6 MeV [8] and 5.28 MeV [9], and to a triton group at $E_x = 10.2$ MeV [8].

Dahlgren *et al.* [10] and Lolos *et al.* [11] also report on ^{10}C excited levels at 3.36 MeV, 5.29 MeV, and 6.61 MeV obtained via the $^9Be(p,\pi^-)^{10}C$ reaction.

In the present $^{10}B(p,n)^{10}C$ charge-exchange study at $E_p = 186$ MeV, we measured the differential cross section

distribution in the angular range between $\theta_{\rm lab} = 0°$ and $\theta_{\rm lab} = 50°$ in steps of $\Delta\theta = 5°$. We also obtained data for the analyzing power A_Y, induced polarization P, and normal polarization transfer coefficient D_{NN} at $\theta_{\rm lab} = 0°$, 15°, and 20°.

This work was motivated in part by the desire to study the $M3$ isovector magnetic transition from the $J^\pi = 3^+$, $T = 0$ ground state of ^{10}B to the $J^\pi = 0^+$, $T = 1$ ground state of ^{10}C. This stretched transition is unique in the sense that it is a g.s. to g.s. transition and that the first excited state in ^{10}C occurs at $E_x = 3.35$ MeV. Reliable cross section measurements over a large range of momentum transfer are therefore allowed. This is not generally the case for other target nuclei, because stretched transitions occur to higher excited states, have small cross sections, and are too weak compared with nearby states to be measured well in a (p, n) reaction. The structure of the spin transition density is uniquely described by a transition density of the form $(p^2_{3/2})_{3^+} \rightarrow (p^2_{3/2})_{0^+}$ with the participating nucleons coupled to maximum angular momentum $J^\pi = 3^+$ for the target ^{10}B(g.s.) wave function [1]. The present data will be compared with results for the ^{10}B$(p, p')^{10}$B($E_x = 1.74$ MeV, 0^+; $T = 1$) analog transition reported in Refs. [3, 4].

Several of the observed ^{10}B$(p, n)^{10}$C transitions are characterized by a large zero-degree cross section. For those transitions, we have estimated the $L = 0$ cross section to obtain the energy distribution of Gamow-Teller (GT) strength that is compared with shell model calculations. Using a simple 1p-1h (one-particle–one-hole) configuration, we also have estimated the location of the dipole and spin-dipole energy distribution that is compared with the data.

II. EXPERIMENTAL SETUP

The experiment was performed using 186 MeV protons from the Indiana University Cyclotron Facility (IUCF) and it was done in two different setups. Differential cross sections measurements were done with an unpolarized proton beam while the polarization observables were measured with a transverse polarized proton beam.

The IUCF swinger neutron time-of-flight (TOF) facility was utilized to perform the experiment. With respect to the undeflected proton beam, two detector stations were located on the 0° and 24° lines, at 101 and 62 m away from the target, respectively. In the first setup for cross section data measurements, each station contained six 102 cm×10 cm×15 cm NE102 scintillator detectors stacked together to form a detector plane placed with its long axis along the beam line (longitudinal configuration). Since the swinger can deflect the trajectory of the incident proton beam to a maximum angle of 26°, the two detector stations were used to cover an angular range between $\theta_{\rm lab} = 0°$ and 50°.

Photomultiplier tubes are located at both ends of each scintillator. The time difference between the signals from the two ends of a scintillator is used to determine the position of the scintillation along the 1 m length. The typical time resolution is about 250 ps. With the neutron detectors in the longitudinal configuration [12], the position information is used to determine the effective flight path for each event with an uncertainty of about 3 cm. With the neutron detectors in the transverse configuration [13] used in the measurement of polarization observables, the position information is used in the determination of the n-p scattering angle for the analyzing event.

The cyclotron radio frequency (RF) signal is used as a STOP signal for TOF determination. Phase drifts of the beam with respect to the RF may be as large as a few nanoseconds. Therefore, a phase drift compensation system is used. The actual phase of the proton beam is sensed with an electromagnetic pickup, and an RF signal locked to this phase is used to generate the stop pulses. This technique keeps the RF in phase with the beam to within 0.5 ns.

Overall neutron energy resolutions were observed to be about 1 MeV in the 0° detector station at 101 m, and about 1.5 MeV in the 24° station at 62 m.

The polarization observables were measured with the IUCF polarimeter [13]. The detectors are stacked to form two parallel planes 100 cm apart, each with six detectors perpendicular to the flight path (transverse configuration). The flight path was 76.5 m. A valid event consists of a neutron scattered from hydrogen in the first plane (called the analyzer) and detected again in the second plane (called the catcher). Back angle n-p scattering in which the proton goes forward has a very low analyzing power at this energy, so such events are not used. A thin, charged-particle detector in front of the catcher is used to distinguish forward- from back-angle scattering. With the detector's capability to obtain the event location, and by keeping track of which detector is triggered, the (x, y) coordinates of the scattering points in both planes are determined and the scattering angles (θ, ϕ) are evaluated. Software cuts can then be easily implemented, during data acquisition or replay, so as to achieve the best figure of merit (FOM) [13] of the polarimeter. With the swinger in use, three data sets for the normal polarization transfer coefficient (D_{NN}), the analyzing power (A_Y), and the induced polarization (P) were taken at $\theta_{\rm lab} = 0°$, 15°, and 20°.

Although the calibration procedures balance the left and right efficiencies of the polarimeter reasonably well, perfect symmetry is never achieved. In addition, at nonzero degree scattering angles, the neutron intensity and polarization may vary with scattering angle so that the intensity and spin might not be the same over the extent of the face of the polarimeter, introducing a left-right asymmetry in the events that is not due to the spin being measured. It is, therefore, necessary to evaluate the instrumental asymmetry. We do this by periodically reversing the spins of the neutrons impinging on the polarimeter. At zero degrees this is easily accomplished by reversing the polarization of the proton beam, because the geometrical symmetry ensures that reversing the proton spin also reverses the neutron spin. At nonzero scattering angles this simplicity no longer holds. The spin-orbit interaction in the scattering potential can induce polarization that depends on the scattering angle. We, therefore, use a superconducting solenoid in the

neutron flight path to reverse the spin of the neutron. In order to reduce the field strength required, we precess the spin 90° rather than 180°. The solenoid polarity is reversible, so we precess the neutron spin 90° left and then 90° right on a periodic cycle. This results in a horizontal spin axis. Since the position resolution along the length of the detectors is about 3 cm and the width of the detectors is 15 cm, we mount the detectors with their long dimension vertical when we use the polarimeter in this mode. The driving current for the solenoid was kept at about 140 A that precessed the spin 90° for 185 MeV neutrons. For lower energy neutrons, a small correction for over-precession was applied, which, e.g., was 0.2% for 170 MeV neutrons.

A low-energy polarimeter, located between the injector cyclotron and the main cyclotron, and two polarimeters located in the high-energy beam lines were used to continuously monitor the proton beam polarization. A typical proton beam polarization of 70% was obtained, with variations under 3% during the experiment period. Spin-up and spin-down polarizations were very well balanced, with a difference less than 0.5%.

III. ANALYSIS OF DATA

Several instrumental calibration procedures were done prior to data reduction. Among these are the calibrations for pulse height, for longitudinal position of an event, and for time of flight for each one of the detectors.

Cosmic ray pulses were used for some of the calibration processes listed above. A cosmic ray event is defined by an event coincidence of all six detectors. The energy loss of cosmic rays in each scintillator is about 33 MeV. The pulse height gain on each detector is thereby calibrated by matching the pulse height peaks of cosmic rays in all detectors. By a least-squares fitting of the cosmic-ray-event positions in all detectors to a straight path, a fine adjustment of the offsets for the event positions is accomplished. Also, a least-squares track fitting in time is used to obtain the relative timing between detectors. The overall time-of-flight calibration was obtained by measuring the $^{13}C(p,n)^{13}N$ reaction with well-known excited states. In each spectrum a small residual cosmic ray background was subtracted. To obtain yields for the observed peaks, a Gaussian peak fitting was implemented. A skewed Gaussian peak was used to simulate the instrumental response funtion. The width and asymmetry of the peak were determined by fitting to the peak shape of $^{10}B(p,n)^{10}C$ ground-state transition at 15°, 20°, and 25° where the peak is well developed as well as completely resolved. The FWHM of the peaks was determined to be 1.0 MeV for spectra obtained in the first detector station, and 1.5 MeV for spectra obtained in the second station. The final results for the differential cross sections were obtained by also taking into account neutron air attenuation effects in the flight path to both detector stations. Moreover, on the second station at 24° the neutron attenuation of a 2 cm copper plate was also included; this plate was used to stop high energy elastically scattered protons short of the neutron detectors. For the cross section measurements two ^{10}B targets of 94.5 mg/cm^2 and 193.5 mg/cm^2 were used. These self-supporting targets were made at IUCF using boron powder enriched to 95.4% in ^{10}B, bound with <2% (in weight) of polyethylene. The 5% ^{11}B in the target produced small contaminant neutron groups. The $^{11}B(p,n)^{11}C$ cross section was also measured with a ^{11}B target of 97.2% purity, so that a proper ^{11}B subtraction could be made in every ^{10}B spectrum. The small contribution due to carbon contamination (in the polyethylene) did not affect the present results for the low-lying states [due to the high negative Q value for the $^{12}C(p,n)^{12}N$ ground-state transition]. The $^{12}C(p,n)^{12}N$ reaction was also measured, with the same setup.

The calibration of solid angle, detector efficiency, and neutron air attenuation were achieved by measuring and normalizing the data to the well-known 0° differential cross section, $\sigma_{c.m.}(0°) = 26.3 \pm 0.8$ mb/sr, of the $^7Li(p,n)^7Be$(g.s.+0.43 MeV) [14]. In this experiment, the measured differential cross section for $^7Li(p,n)^7Be$(g.s.+0.43 MeV) at all angles between $\theta_{lab} = 0°$ and 50° agrees very well with previously reported values [14].

In Fig. 1 we present spectra obtained at $\theta = 0°$, 10°, and 15° for the $^{10}B(p,n)^{10}C$ reaction. The measured time-of-flight spectra, after correction for the ^{11}B admixture in the target, have been converted to an energy spectra. The ground state and the 3.35 MeV state are clearly visible as well as neutron groups at $E_x = 5.3$, 9.0, 10.0, and 16.5 MeV, indicated in Fig. 1 by vertical arrows.

In the second setup used to measure spin observables a self-supporting target made with 99.5% enriched ^{10}B of 205.4 mg/cm^2 and a polarized proton beam were used.

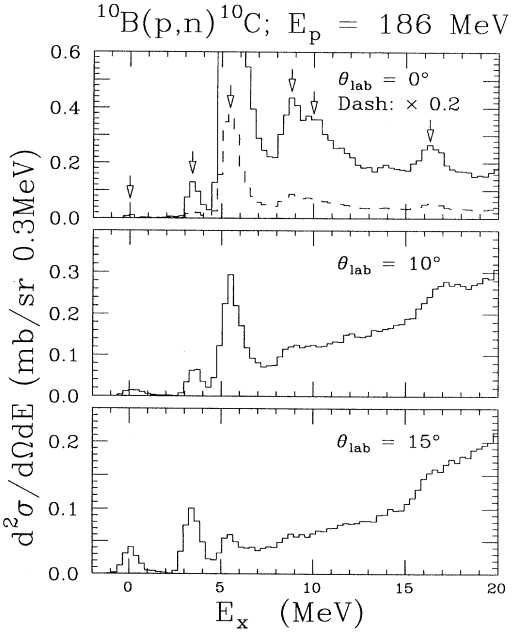

FIG. 1. Neutron energy spectra for the $^{10}B(p,n)^{10}C$ reaction at $\theta_{lab} = 0°$, 10°, and 15°, and $E_p = 186$ MeV. In the dashed curve, the $\theta_{lab} = 0°$ spectrum is shown scaled by a factor of 0.2. Vertical arrows indicate neutron groups at $E_x = 0$, 3.35, 5.3, 9.0, 10.0, and 16.5 MeV.

Values for D_{NN}, A_Y, and P, were measured at $\theta_{\rm lab} = 0°$, 15°, and 20°.

The following relation holds at a given angle for these observables:

$$p_f[1 + p_i A_Y(\theta)] = P(\theta) + p_i D_{NN}(\theta)\,, \tag{3.1}$$

where p_i and p_f are respectively the incident proton beam polarization and the final polarization of the scattered neutrons at the scattering angle θ. Similar instrumental calibrations were done as in the cross section measurement setup. However, an additional calibration was done to obtain the effective analyzing power (A_E) of the polarimeter. This was necessary to determine p_f. The calibration of A_E was done at $\theta_{\rm lab} = 0°$ by using the GT transition in the ^{6}Li$(p,n)^6$Be(g.s.) reaction which has been measured at $E_p = 200$ MeV to have, at $\theta = 0°$, a value $D_{NN} = 0.333 \pm 0.021$ [15]. From Eq. (3.1) it follows that, at $\theta = 0°$,

$$p_f = p_i D_{NN}(0°)\,, \tag{3.1$'$}$$

because $A_Y(0°) = P(0°) = 0$. Thus, the p_f value may be easily determined, assuming that the value for D_{NN} is known and that p_i is measured with the beam line polarimeter. The following relation [13] between the neutron polarization p_f and the effective analyzing power of the polarimeter A_E is used to obtain A_E:

$$p_f(0°) = \frac{1}{A_E}\frac{(R-1)}{(R+1)}\left[1 - \frac{(R-1)^2}{4R}(\delta p_i/p_i)^2\right]. \tag{3.2}$$

The quantity R, which reflects the observed left-right asymmetry, is defined as

$$R^2 = \frac{N(L^+)N(R^-)}{N(L^-)N(R^+)}\,, \tag{3.3}$$

where $N(L^\pm)$ refers to the number of left-scattering neutrons on the polarimeter when the proton beam spin was oriented up/down ($\pm$), and similarly for $N(R^\pm)$ except for right scattering. In Eq. (3.2) a correction has been made up to second order in the quantity $\delta p_i/p_i$ which is nonzero when the polarizations for spin up (p_i^+) and spin down (p_i^-) are unbalanced, with $p_i \equiv (p_i^+ - p_i^-)/2$ and $\delta p_i \equiv (p_i^+ + p_i^-)/2$. However, the measured $\delta p_i/p_i$ in this experiment was less than 1% and the second-order term in Eq. (3.2) is negligible. Thus, Eq. (3.2) is simplified as

$$p_f(0°) = \frac{1}{A_E}\frac{(R-1)}{(R+1)}\,. \tag{3.4}$$

The average value obtained for A_E in this experiment was $A_E = 0.320 \pm 0.022$. This value is consistent with measured values previously reported using the same apparatus [13].

For nonzero degree scattering angles, the use of the superconducting solenoid is essential to obtain reliable results. The following quantities were determined directly from the measurements:

$$(R^+)^2 = \frac{N(L^{++})N(R^{+-})}{N(L^{+-})N(R^{++})}\,, \tag{3.5a}$$

$$(R^-)^2 = \frac{N(L^{-+})N(R^{--})}{N(L^{--})N(R^{-+})}\,, \tag{3.5b}$$

where the first + (−) refers to the proton spin up (down) direction and the second + (−) refers to the right-hand (left-hand) solenoid precession direction. We denote, for proton spin up,

$$p_f^+ = \frac{1}{A_E}\frac{(R^+-1)}{(R^++1)}\,, \tag{3.6}$$

and for proton spin down,

$$p_f^- = \frac{1}{A_E}\frac{(R^--1)}{(R^-+1)}\,. \tag{3.7}$$

Then, we define

$$p_f \equiv (p_f^+ - p_f^-)/2 = \frac{(R^+ - R^-)}{A_E(R^++1)(R^-+1)} \tag{3.8}$$

and

$$\delta p_f \equiv (p_f^+ + p_f^-)/2 = \frac{(R^+R^- - 1)}{A_E(R^++1)(R^-+1)}\,. \tag{3.9}$$

Spin-up and spin-down cross sections can be calculated using

$$\sigma^+ \equiv \frac{(\sigma^{++}) + (\sigma^{+-})}{2} = C_1[N(L^{++}) + N(R^{++})] + C_2[N(L^{+-}) + N(R^{+-})]\,, \tag{3.10a}$$

$$\sigma^- \equiv \frac{(\sigma^{-+}) + (\sigma^{--})}{2} = C_1[N(L^{-+}) + N(R^{-+})] + C_2[N(L^{--}) + N(R^{--})]\,, \tag{3.10b}$$

where C_1 and C_2, with the factor 2 absorbed, are the normalization constants involving computer and electronics live time and total beam charge. We define the ratio r, which indicates the spin-up and spin-down asymmetry, as

$$r \equiv \frac{\sigma^+}{\sigma^-}\,. \tag{3.11}$$

With the values determined above, the polarization observables are calculated by the following equations [13] for nonzero degree scattering angles:

$$A_Y(\theta) = \frac{1}{p_i}\frac{(1-r)}{(1+r)}\left[1 + \frac{\delta p_i(1-r)}{p_i(1+r)}\right]^{-1}, \tag{3.12a}$$

$$D_{NN}(\theta) = p_i^{-1}[p_f - (p_f\delta p_i + p_i\delta p_f)A_Y(\theta)], \tag{3.12b}$$

$$P(\theta) = p_i^{-1}[(p_f\delta p_i - p_i\delta p_f) + p_f(p_i^2 - \delta p_i^2)A_Y(\theta)]. \tag{3.12c}$$

IV. RESULTS

In this section we present results obtained for transitions to resolved final states in ^{10}C and results from a

multipole decomposition analysis [16] in the excitation energy region above 6 MeV. The experimental results are compared with distorted-wave impulse approximation (DWIA) calculations.

A. Distorted-wave impulse approximation calculations

We used the computer code DW81 [17] for the microscopic DWIA calculations. In these calculations, the knock-out exchange amplitudes are treated exactly.

The distorted waves were calculated using optical-model potential (OMP) parameters obtained by Lewis *et al.* [3] in the analysis of elastic scattering of 200 MeV protons from ^{10}B. These parameters were adjusted to the appropriate nucleon energy using the energy dependence suggested in the p+^{12}C analysis between 20 and 200 MeV by Comfort and Karp [18]. In Ref. [3], the real central part of the OMP is represented as the sum of an attractive Woods-Saxon and a repulsive surface-peaked Gaussian contribution. In our analysis we replaced the Gaussian contribution by a first derivative Woods-Saxon form, such that both have the same volume integral. However, the calculated ^{10}B(p,n)^{10}C results were rather insensitive to this term of the OMP. An asymmetry potential of $23.5(N-Z)/A$ MeV was included in the OMP for the outgoing n+^{10}C channel. Other choices of OMP parameters such as those described in Ref. [4] were also used, which resulted in less than a few percent variation in the calculated inelastic cross section values.

For the interaction between the incident and struck nucleons, we used the free nucleon-nucleon interaction as parametrized by Franey and Love [19] at $E = 210$ MeV.

The other ingredients needed in the calculation of the inelastic differential cross sections are the one-body density matrix elements (OBDME's) obtained from a suitable nuclear structure calculation and a prescription to calculate the single-particle wave functions for the nucleons participating in the transition. Harmonic oscillator (HO) wave functions were assumed for the single-particle wave functions. The nucleus ^{10}B is a light nucleus, and, as such, center-of-mass corrections are important. These were done as described by Millener in the Appendix of Ref. [20]. A reduced HO parameter size, $b_r = [\frac{A}{(A-1)}]^{1/2} b_0$, was used with a nucleus core mass of $(A-1)$. We used the value $b_0 = 1.606$ fm obtained by Hicks *et al.* [1] in their analysis of transverse electron scattering from ^{10}B. In the present analysis, we restrict ourselves to $0\hbar\omega$ and $1\hbar\omega$ shell-model configurations. As such [20], the relative OBDME's are larger than the conventional shell-model OBDME's by a factor $[\frac{A}{(A-1)}]^{Q/2}$, where $Q = Q_1 + Q_2$ is the number of quanta for the two orbits involved in the transition.

The shell-model code OXBASH [21] was used to calculate the 1p-1h OBDME's. These were done in the *spsd* shell-model space. For positive-parity transitions and because the ground state of ^{10}B has a $J^\pi = 3^+$, only 1p-1h $0\hbar\omega$ $p \rightarrow p$ transitions are included. For $1\hbar\omega$, negative 1p-1h transitions between $s \rightarrow p$ and $p \rightarrow sd$ configurations were considered. The OBDME's values were obtained using the Millener and Kurath [22] interaction. The OBDME's values obtained for positive parity transitions agree very well with the values reported by Lee and Kurath [2] for the first 3 states in ^{10}C. The excitation energies of $T = 1$ states up to 10 MeV excitation, in $A = 10$ isobars, from the present shell-model calculations are compared in Fig. 2 with empirical data from the compilation by Ajzenberg-Selove [23]. Among the calculated low-lying levels, the first two negative parity states, 1^- and 2^-, are about 3 MeV higher than empirically observed in ^{10}B. A calculation including up to $2\hbar\omega$

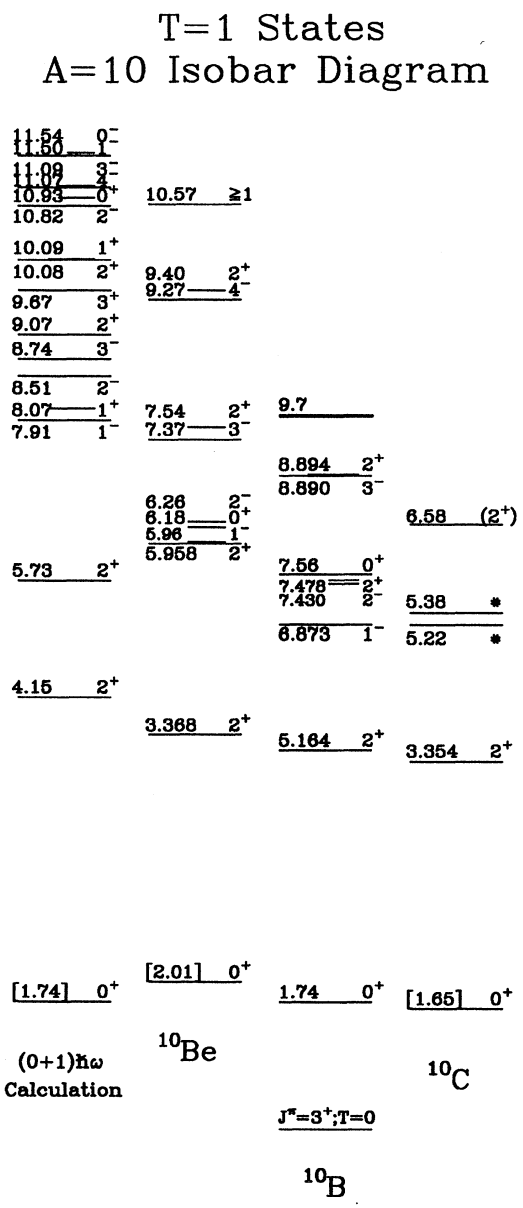

FIG. 2. Energy level diagram for $A = 10$, showing only $T = 1$ states. Experimental information on states in ^{10}Be, ^{10}B, and ^{10}C [23] are compared with shell model calculations. One of the two ^{10}C states labeled with an asterisk is presumably the 2_2^+ state.

configuration [24] gives a better agreement for these negative parity states. It also gives a similar agreement for positive parity states as that shown in Fig. 2 with the present calculation.

B. Transitions to low-lying states in ^{10}C

1. The $^{10}B(3^+, g.s.) \rightarrow ^{10}C(0^+, g.s.)$ transition

An $M3$ transition from the ^{10}B(g.s.) to the ^{10}C(g.s.) induced by a one-body operator between p shell model wave-function states with $\Delta n = 0\hbar\omega$ can only proceed through the stretched $(p^2_{3/2})_{3+}$ configuration. This transition, in which both spin and isospin are transferred, is mainly sensitive to the tensor isovector components of the nucleon-nucleon (NN) interaction. Previous studies with (e, e') scattering experiments [1] indicate that $1p_{3/2}$ nucleons provide an excellent representation of the transition density. Therefore, with well-characterized wave functions, the ^{10}B(g.s.) to ^{10}C(g.s.) transition is a unique case to test up to large momentum transfer the spin-isospin terms in the NN interaction.

The measured differential angular distribution up to a momentum transfer $q = 2.5$ fm^{-1} is presented in Fig. 3; for comparison purposes we also include the ^{10}B$(p, p')^{10}$B(1.74 MeV) data to the analog 0^+ transition in ^{10}B, as reported by Lewis *et al.* [3] (square symbols) and by Baghaei *et al.* [4] (crosses). The ^{10}B$(p, p')^{10}$B(0^+, $T = 1$) cross section and the ^{10}B$(p, n)^{10}$C(0^+) cross section at the same bombarding energy are simply related via a Clebsch-Gordan coefficient, assuming unbroken isospin symmetry. In this case the Clebsch-Gordan coefficient has a value of 2 and the reported ^{10}B$(p, p')^{10}$B(0^+, $T = 1$) cross sections have been multiplied by this factor. As shown in Fig. 3, there is good agreement among the three measurements if the cross sections are plotted as a function of momentum transfer, q. The data of Lewis *et al.* [3] seem to be somewhat larger than the other two sets of data near the maximum ($q \sim 1.1$ fm^{-1}) of the angular distribution, although it agrees well for q values above 1.5 fm^{-1}. We also present in Fig. 3 several curves describing DWIA calculations in which just the tensor term (solid line) or just the central term (dot-dashed) or just the spin-orbit term (dashed) of the effective NN interaction have been included. The coherent sum of all terms of the effective NN interaction is presented as a dotted curve. The importance of the tensor interaction for $1 < q < 2$ fm^{-1} is clearly noted. The magnitude and shape of the empirical cross section are well reproduced by the calculations, and no adjustment was needed for any of the parameters involved.

In Fig. 4 we display the spin observables measured for this transition up to $q = 1.25$ fm^{-1}. Values for A_Y, P, and D_{NN} that overlap with the present measurements, measured by Baghaei *et al.* [4] for the analog transition in the ^{10}B(p, p') reaction, are also displayed in Fig. 4 (crosses). These measurements show a very good agreement. Two theoretical calculations are also shown. The dashed curve is a plane wave impulse approximation (PWIA) calculation while the solid line represents a full DWIA calculation. The authors of Ref. [4] indicate that while their reported data in the range of q up to 3 fm^{-1} for differential cross section, A_Y and P observables are reasonably described by calculations based on the free nucleon-nucleon t matrix, the D_{NN} data are not. In the limited region which our present data span, $0 < q < 1.2$ fm^{-1}, we observe good agreement between

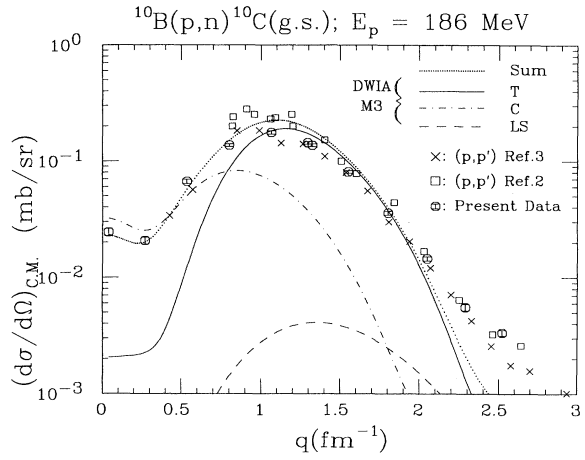

FIG. 3. Values for differential cross section data (octagons) for the ^{10}B$(p, n)^{10}$C(g.s.) reaction at $E_p = 186$ MeV are presented versus momentum transfer q. Published data for the analog transition ^{10}B$(p, p')^{10}$B(1.74, 0^+, $T = 1$), obtained at $E_p = 200$ MeV from Refs. [3] (squares) and [4] (diagonal crosses), have been multiplied by 2 to compare with present results. The curves are $M3$ DWIA calculations (see text), using only tensor interaction (solid line), central interaction (dot-dashed), or spin-orbit interaction (dashed), with the coherent sum of all terms of the effective interaction shown as a dotted curve.

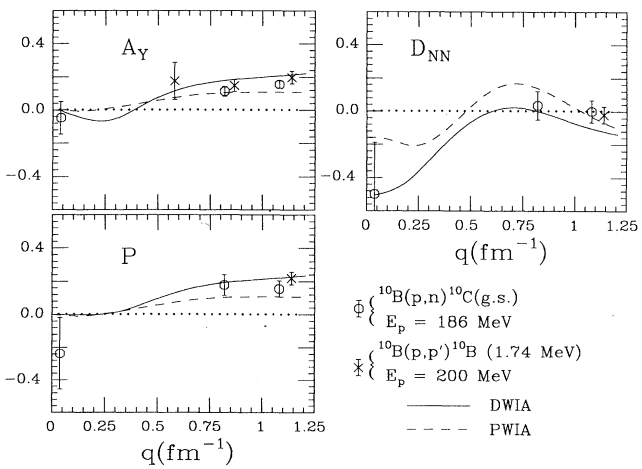

FIG. 4. Analyzing power A_Y, polarization P, and normal polarization transfer D_{NN} data obtained at $E_p = 186$ MeV are presented for the $M3$ ^{10}B$(p, n)^{10}$C(g.s.) transition versus momentum transfer q. Data from Ref. [4], obtained for the analog transition ^{10}B$(p, p')^{10}$B(1.74, 0^+, $T = 1$) at $E_p = 200$ MeV are shown as crosses. The curves are PWIA (dashed) and DWIA (solid line) calculations.

data and DWIA calculations.

In the PW approximation the values of D_{NN} are related to the ratio of the transverse spin ($\bar{v}_\tau^t = \bar{v}_{\sigma\tau}^c + \bar{v}_\tau^T$) and longitudinal spin ($\bar{v}_\tau^\ell = \bar{v}_{\sigma\tau}^c - 2\bar{v}_\tau^T$) couplings which are combinations of the isovector central, $\bar{v}_{\sigma\tau}^c$, and isovector tensor, $\bar{v}_\tau^T$, components of the NN interaction including knockout exchange terms [25]. Neglecting the small spin-orbit and tensor exchange interference terms, D_{NN} may be expressed as

$$D_{NN} \approx -\left[1 + \left|\frac{\rho_J^t \bar{v}_\tau^t}{\rho_J^\ell \bar{v}_\tau^\ell}\right|^2\right]^{-1} \quad (4.1)$$

where ρ_J^t and ρ_J^ℓ are the transverse and longitudinal nuclear transition densities and J is the total angular momentum transfer. Baghaei *et al.* [4] point out that for stretched transitions $|\rho_J^t/\rho_J^\ell|^2 = (J+1)/J$, and thus D_{NN} in the PW approximation is directly related to the relative strength of the transverse and longitudinal spin components of the effective NN interaction. In this approximation, empirical values of $D_{NN}(q)$ may be directly related to the ratio $\bar{v}_\tau^t(q)/\bar{v}^\ell(q)$, for values of q near the maximum of the differential cross section.

We show in Fig. 4 the calculated DWIA and PWIA results for D_{NN}. First we note that the two curves are not the same, particularly at low q, indicating that at this bombarding energy distortion effects are important in that region and second that the present empirical D_{NN} results are in fair agreement with the DWIA calculations.

2. The $^{10}B(p,n)^{10}C(3.35\ MeV,\ 2_1^+)$ transition

The transition to the known 2_1^+ state [23] in ^{10}C is a $3^+ \rightarrow 2^+$ transition and as such it consists of an incoherent admixture of a Gamow-Teller (GT) transition ($\Delta J = 1^+$), a quadrupole transition ($\Delta J = 2^+$), and an $M3$ transition ($\Delta J = 3^+$). The measured differential cross sections are presented versus momentum transfer, q, in Fig. 5. There are no ^{10}B$(p,p')^{10}$B reported data for the analog transition in Refs. [3, 4]. We have used the OBDME, obtained with the code OXBASH, to calculate the different ΔJ^π contributions. These OBDME have similar values to those obtained using the Lee and Kurath's wave functions [2]. The DWIA results are indicated in Fig. 5. The $\Delta J = 1^+$ (GT) calculated differential cross section had to be normalized by 0.15. No rescaling was needed for the quadrupole component, while a normalization factor of 1.03 was used for the calculated $M3$ transition. The normalization used for the GT transition indicates that the Lee and Kurath wave functions overestimate the GT contribution to this 2_1^+ state by about a factor of 6. A similar large discrepancy for a GT transition has been reported by Goodman *et al.* [26] in the ^{13}C$(p,n)^{13}$N(3.51 MeV) transition. The $\Delta J^\pi = 1^+$ cross section extrapolated to $(q,w) = (0,0)$ yields a value of $\sigma_{GT} = 0.28 \pm 0.01$ mb/sr which corresponds to a value $B(\mathrm{GT}) = 0.03$ (see Sec. IV D).

The measured polarization observables are presented in Fig. 6 together with PWIA and DWIA calculations obtained using the weighing factors for the individual transitions indicated in Fig. 5. A good agreement is observed between the DWIA calculations and data.

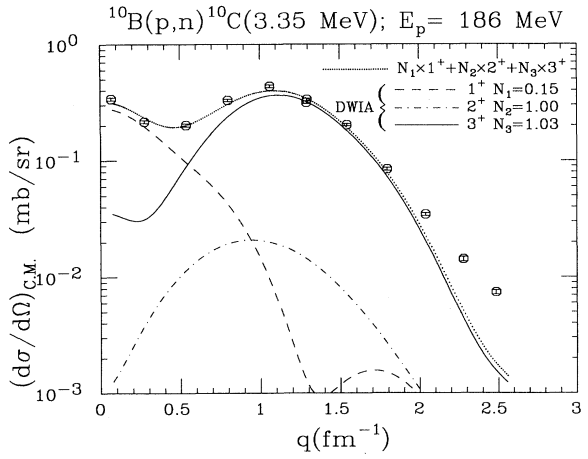

FIG. 5. Differential cross section data for the ^{10}B$(p,n)^{10}$C(2^+, 3.35 MeV) transition at $E_p = 186$ MeV are presented versus momentum transfer q. The curves are DWIA calculations (see text). The calculated differential cross sections for $\Delta J^\pi = 1^+$ (dashed) and 3^+ (solid line) have been normalized respectively by a factor of $N_1 = 0.15$ and $N_3 = 1.03$. The 2^+ contribution (dot-dashed) needs no normalization. The incoherent sum is shown by the dotted curve.

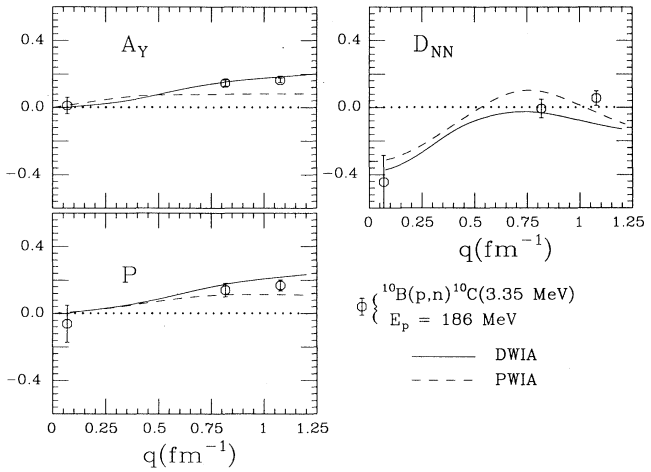

FIG. 6. Analyzing power A_Y, polarization P, and normal polarization transfer D_{NN} data obtained at $E_p = 186$ MeV are presented for the ^{10}B$(\vec{p},\vec{n})^{10}$C(2^+, 3.35 MeV) transition versus momentum transfer q. The curves are PWIA (dashed) and DWIA (solid line) calculations, obtained using the normalization values indicated in Fig. 5.

3. The $^{10}B(p,n)^{10}C(5.3\ MeV)$ transition

Two states, one of which is presumably the 2_2^+ state, are reported by Ajzenberg-Selove [23] at 5.22 ± 0.04 MeV and 5.38 ± 0.07 MeV in ^{10}C. In the mirror nuclei ^{10}B, the 2_2^+ state is reported at $5.958\,39 \pm 0.000\,05$ MeV while negative parity states are reported at 5.9599 ± 0.0006 MeV

($J^\pi = 1^-$) and 6.1793 ± 0.0007 MeV ($J^\pi = 2^-$). The shell-model calculations also predict 1^- and 2^- states close to the 2_2^+ (see Fig. 2).

We have analyzed the neutron group observed at this excitation energy, and the measured angular distribution is presented versus momentum transfer in Fig. 7. We have used the OXBASH 1p-1h OBDME to calculate the DWIA differential cross sections for transitions to the 2_2^+, 1_1^-, and 2_1^- states that constitute this neutron group. The contributions from positive (solid curve) and negative (dashed curve) transitions are shown in Fig. 7. The incoherent sum of all transitions is shown as a dotted curve. It is clear from Fig. 7 that the measured zero-degree cross section (see also Fig. 1) is dominated by the $\Delta J^\pi = 1^+$ contribution to the 2_2^+ transition, with a rather small cross section contribution due to the negative parity states.

In order to *estimate* the cross section to the 2_2^+ state in ^{10}C we have *subtracted* the DWIA calculated cross sections to the 1_1^- and 2_1^- states from the measured cross sections to the neutron group at 5.3 MeV. The results are shown in Fig. 8; the error bars reflect the statistical uncertainties as well as estimated uncertainties in the calculated cross sections.

In the DWIA analysis for the $3^+ \rightarrow 2_2^+$ transition, we had a similar problem to the one we have studied in the DWIA analysis of the $\Delta L = 0$ transitions for the ^{6}Li$(p,n)^6$Be(g.s.) [15] and in the ^{13}C$(p,n)^{13}$N(g.s.) [27] reactions. In Ref. [27] we indicated that the $\Delta L = 0$ GT transition to the 3.51 MeV excited state in ^{13}N is well reproduced by the standard DWIA calculations. However, the $\Delta L = 0$ mirror transition to the ground state of ^{13}N with a much steeper slope needed some adjustment. In particular, a larger HO size parameter for the bound-state wave function was needed to describe the data properly. In the present case we have a similar situation. The $\Delta J = 1^+$ contribution to the 3.35 MeV transition in ^{10}C seems to be well reproduced by the DWIA calculations with the standard parameters indicated in Sec. IV A (see Fig. 5). However, the $\Delta L = 0$ component in the transition to the 5.3 MeV neutron group has a much steeper slope for momentum transfer values in the range $0 < q < 1$ fm^{-1} (Fig. 7) than the transition to the 3.35 MeV state. In order to have a reasonable description to the $\Delta J = 1^+$ contribution to the data represented in Fig. 7 and Fig. 8, we have used a larger HO size parameter, $b_r = 2.6$ fm. Calculations for all other transitions were done with the standard value $b_r = 1.693$ fm. Nuclear structure reasons for the striking difference in the shape of the cross section distributions for the first two excitations in the ^{13}C$(p,n)^{13}$N reaction are presented in Ref. [27]. Since the transitions involved in all these cases are all $1p$ shell model transitions, we believe the reasons are the same and, furthermore, it may denote similarities in the wave function of the states involved.

This 3^+ to 2_2^+ transition also consists of incoherent admixtures of GT transition ($\Delta J = 1^+$, solid curve), quadrupole transition ($\Delta J = 2^+$, dot-dashed curve), and $M3$ transition ($\Delta J = 3^+$, dashed curve). These DWIA calculations plus the incoherent sum (dotted curve) are shown in Fig. 8. In this case the calculated differential cross sections were normalized by 0.51 for the GT and quadrupole transition and 0.41 for the $M3$ transition. The factor 0.51 needed for the GT transition indicates that the Lee and Kurath wave functions [2] overpredict the GT contribution to this 2_2^+ state by almost a factor of 2. The $\Delta J = 1^+$ component to the differential cross section to the 2_2^+ state extrapolated to ($q = w = 0$) yields

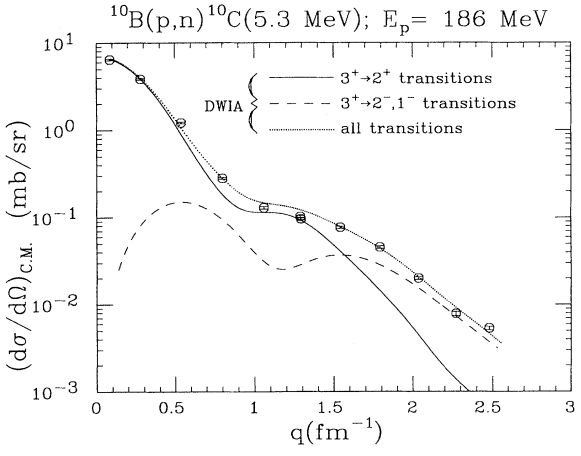

FIG. 7. Differential cross section data for the neutron group at $E_x = 5.3$ MeV in the ^{10}B$(p,n)^{10}$C reaction at $E_p = 186$ MeV. In addition to the 2_2^+ state, theoretical predictions show that this neutron group includes transitions to a 1^- state and a 2^- state that cannot be resolved in this experiment. The solid curve corresponds to incoherent summation of different ΔJ^π components for the 3^+ to 2_2^+ transition calculated with DWIA. The dashed curve corresponds to the incoherent sum of transitions from the 3^+ to both 1^- and 2^- states. The dotted line is the total calculated distribution.

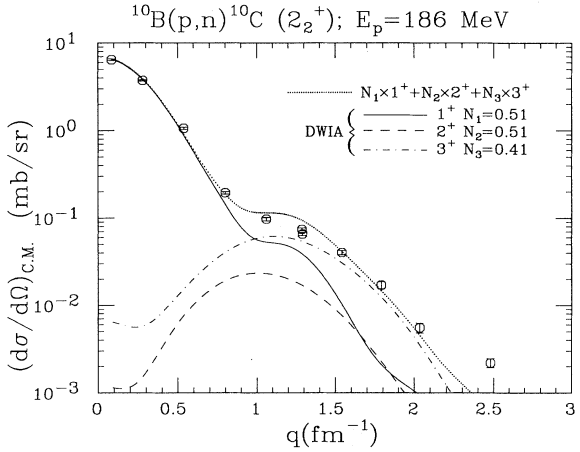

FIG. 8. Estimated differential cross section for transition to the 2_2^+ state, data obtained by subtracting the negative parity contribution from the $E_x = 5.3$ MeV neutron group (see Fig. 7). The DWIA calculations for different ΔJ^π components have been normalized as indicated and then summed incoherently to fit the data.

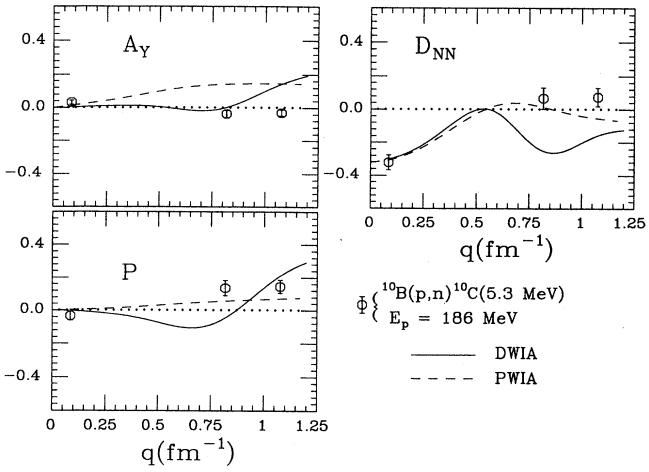

FIG. 9. Analyzing power A_Y, polarization P, and normal polarization transfer D_{NN} data obtained at $E_p = 186$ MeV are presented for the neutron group at 5.3 MeV in the ^{10}B$(\vec{p},\vec{n})^{10}$C reaction versus momentum transfer q. The curves are PWIA (dashed) and DWIA (solid line) calculations.

a value $\sigma_{GT} = 6.44 \pm 0.14$ mb/sr, which corresponds to a $B(GT) = 0.68 \pm 0.02$ (see Sec. IV D). It should be noted that the value of the calculated zero-degree cross section for the $\Delta J = 1^+$ transition is not too sensitive to the value of b_r. It increased less than 5% for the higher b_r value used for the GT transition.

The polarization observables obtained for the neutron group at 5.3 MeV are presented in Fig. 9. Except for the A_y values, the other observables have similar values to those obtained for the 2_1^+ transition and are fairly reproduced by the DWIA calculations. In these calculations an incoherent sum of all transitions involved with the same weighting factors of Fig. 7 have been used. For completeness we also present in dashed curves the results of PWIA calculations.

4. Other $^{10}B(p,n)^{10}C$ transitions

A state in ^{10}C at about 6.6 MeV is reported [23] to be excited in the ^{9}Be(p,π^-), ^{10}B$(^3$He$,t)$, and ^{12}C(p,t) reactions. It is presumably the analog of the 2_3^+ state at 7.542 $\pm$ 0.001 MeV in ^{10}Be [23]. From the zero-degree spectrum (Fig. 1) it seems that the ^{10}B$(p,n)^{10}$C(6.6 MeV, 2_3^+) transition has a weak $\Delta J^\pi = 1^+$ component. No angular distribution was obtained for this transition.

Neutron groups at around 9 MeV excitation are observed in the zero-degree spectrum (Fig. 1), indicating a concentration of GT strength at that energy. However, because of the large density of states and the achieved energy resolution, no attempt was made to obtain individual transitions. Instead we have done a multipole decomposition analysis of the data for unresolved states up to 30 MeV excitation energy (see Fig. 10).

The neutron group centered at around 16.5 MeV excitation in ^{10}C (see 0° spectrum in Fig. 1) represents another concentration of GT strength that we believe corresponds to the excitation of the analog 2^+ resonance in ^{10}B reported at $E_x = 18.8$ MeV [23]. This resonance in ^{10}B has been reported in the ^{7}Li$(^3$He$,\gamma)^{10}$B reaction and in the ^{7}Li$(^3$He$,\alpha)^6$Li excitation function at $E(^3$He$) = 1.4$ MeV. Similarly 2^-, $T = 1$ resonances in ^{10}B are also reported at 18.43 and 19.29 MeV and a 1^-, T=1 resonance at 20.1 MeV [23]. The analogs of these resonances in ^{10}C are clearly seen in the present (p,n) study (see Fig. 10). The 1p-1h shell-model calculations using the code OXBASH indicate that transitions to these 2^- and 1^- states have mainly $1d_{3/2}$-$1p_{3/2}$ and $2s_{1/2}$-$1p_{3/2}$ configurations.

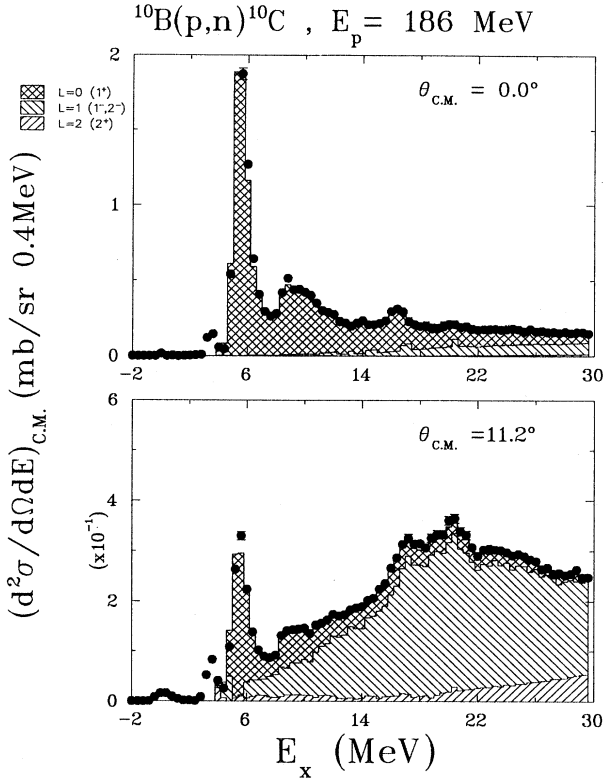

FIG. 10. Multipole decomposed spectra for the ^{10}B$(p,n)^{10}$C reaction at $\theta_{c.m.} = 0°$ and 11.2°. The multipole analysis spectra start at $E_x = 4.0$ MeV. Experimentally observed cross sections are displayed as solid circles with error bars representing the statistical uncertainties. Cross sections with different orbital angular momentum transfer, characterized by $L = 0$, 1, and 2, are decomposed and illustrated with different shadow patterns.

C. Multipole decomposition analysis

The obtained ^{10}B$(p,n)^{10}$C spectra (Fig. 1) indicate that the density of states above 7.0 MeV excitation in ^{10}C is large, which combined with the obtained 1.0 MeV energy resolution does not allow an immediate identification of individual transitions. To be able to extract further information from the data, we present a multipole decomposition analysis (MDA) of the data, as de-

scribed in Refs. [16] and [28]. In this approach we bin the center-of-mass double differential cross section data in 0.5 MeV excitation energy steps for angles between $\theta_{\rm lab} = 0°$ and 20° which are fitted, with DWIA outputs also prepared in 0.5 MeV intervals, using a least-squares fitting technique.

The shapes of the calculated angular distributions are characterized by ΔJ^π transfers. We have calculated these shapes for all possible 1p-1h configurations with final J^π states 0^+, 0^-, 1^+, 1^-, 2^+, 2^-, 3^+, 3^-, and 4^-. The strength of each 1p-1h configuration for a transition to a given eigenstate was calculated with the OXBASH shell-model code. We have chosen the p-h configuration with the largest OBDME amplitudes to represent each ΔJ^π transition in the MDA. Since the shape of the differential cross section changes smoothly with increasing excitation energy E_x, we have done DWIA calculations in 5 MeV excitation energy intervals between 0 and 30 MeV for each p-h configuration. An interpolation routine [28] was used to obtain the necessary shapes in steps of 0.5 MeV.

As noted in Ref. [16], the differences in shape for spin transitions characterized with a given ΔL is not large enough and cannot be determined from the present experimental data. Therefore, we report the results of the MDA by grouping all ΔJ^π transitions that correspond to a given ΔL transfer. Although differential cross sections data were taken up to $\theta_{\rm lab} = 50°$, in this MDA study we are mainly interested in transitions with $\Delta L = 0$, 1 and 2 which above $\theta_{\rm lab} = 25°$ have small cross sections. Thus we decided to use a data set with only five angles, 0°, 5°, 10°, 15° and 20°, to do the MDA fitting with up to four ΔJ^π shapes. In general we included $\Delta J = 1^+(\Delta L = 0)$, $\Delta J = 1^-$, $2^-(\Delta L = 1)$, and $\Delta J = 2^+(\Delta L = 2)$.

Some of the results obtained at $\theta_{\rm lab} = 0°$ and 10° are shown in Fig. 10. A continuous distribution of $\Delta L = 0$ (GT) transitions is observed up to 30 MeV, while the $\Delta L = 1$ strength seems to peak at around 20 MeV of excitation energy. The validity of this MDA approach as previously noted [29] relies on how well-known spin dipole transitions are fitted with the assumed DWIA shapes.

D. Gamow-Teller strength

The Gamow-Teller strengths from the ^{11}B$(p,n)^{11}$C reaction have been studied by Taddeucci *et al.* [30]. Excited states in ^{11}C up to about 14 MeV carry a total $\sum B(\mathrm{GT})_{\rm exp} = 2.56 \pm 0.07$ or 71% of the theoretical value $\sum B(\mathrm{GT})_{\rm thy} = 3.628$ obtained using the Cohen and Kurath [2] transition densities. In the present case, the ground state of the nucleus ^{10}B has a $J^\pi = 3^+$, so that transitions to final states in ^{10}C with $J^\pi = 2^+$ and 3^+ carry GT strength. We have used the code OXBASH [21] to calculate the GT strength in a $0\hbar\omega$ 1p-1h model assuming only $1p$ shell-model transitions. The model predicts a total $\sum B(\mathrm{GT})_{\rm thy} = 2.11$ to excited states up to about 25 MeV of excitation, but 96% of the strength is in states below 10 MeV of excitation. In particular, the model predicts a $B(\mathrm{GT}) = 0.184$ in the $3^+ \rightarrow 2^+_1$ transition, a $B(\mathrm{GT}) = 1.36$ in the $3^+ \rightarrow 2^+_2$ transition, and a $B(\mathrm{GT}) = 0.46$ in the $3^+ \rightarrow 3^+_1$ transition predicted at 9.67 MeV of excitation in ^{10}C. (See Fig. 11).

In transitions to resolved final states, we have estimated the $L = 0$ contribution to the measured differential angular distributions as indicated in Sec. IV B. We use a value $\hat{\sigma} = 9.4$ mb/sr unit GT for the unit GT cross section, to estimate the empirical GT strength from the zero-degree $L = 0$ cross section extrapolated to $(q = w = 0)$. The unit GT cross section value is from Ref. [30], and corresponds to an average value obtained for the ^{11}B$(p,n)^{11}$C(g.s.) transition at $E = 160$ and 200 MeV. Values of $B(\mathrm{GT}) = 0.03$ and 0.69 are estimated for the 2^+_1 and 2^+_2 transitions.

We have used the MDA to obtain the $L = 0$ spectrum (Fig. 10) which has been extrapolated to $(q = w = 0)$ and divided by the unit cross section value to obtain an energy distribution of the GT strength. The results are presented in Fig. 11 together with the empirical GT values to the 2^+_1 and 2^+_2 transitions. We observe up to 10 MeV excitation 1.17 ± 0.15 $B(\mathrm{GT})$ units and 1.9 ± 0.2 $B(\mathrm{GT})$ units up to 20 MeV of excitation. This indicates that up to 10 MeV excitation we obtain only about 58% of the predicted GT strength. The data seems to indicate that the rest of the GT strength is distributed over a larger excitation energy region, which may be predicted with a larger $\hbar\omega$ shell-model calculation.

As indicated above, the amount of $L = 0$ cross section estimated from the MDA depends sensitively on the shape of other multipoles, in particular $L = 1$, angular distributions. In order to obtain the $L = 0$ cross section in a less model-dependent fashion, we used the method suggested by Goodman and Bloom [31]. In this approach, the 10° spectrum is subtracted from the 0°

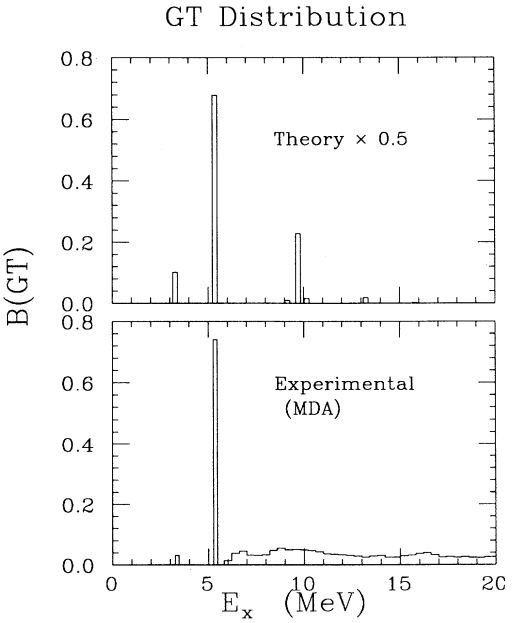

FIG. 11. Energy distribution of GT strength as obtained theoretically from a 1p-1h calculation (top) is compared with the present empirical results (bottom). Above 4.0 MeV of excitation the MDA was used to obtain the GT values.

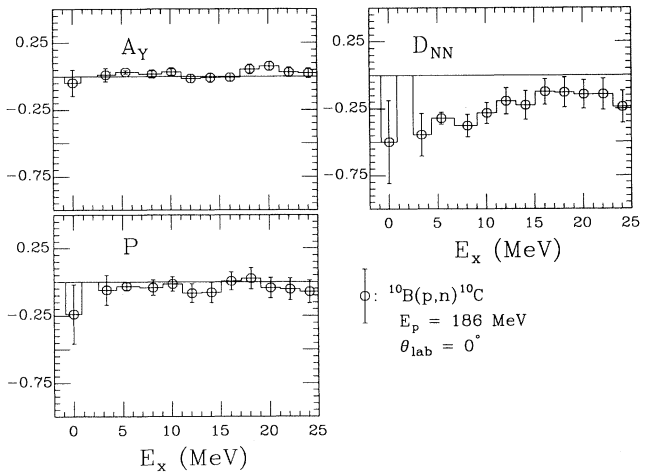

FIG. 12. Data obtained at $\theta_{\rm lab} = 0°$ for the ^{10}B($\vec{p},\vec{n}$)^{10}C reaction at $E_p = 186$ MeV have been binned in 2 MeV bin size to calculate values for the analyzing power A_Y, polarization P, and transverse polarization transfer D_{NN}.

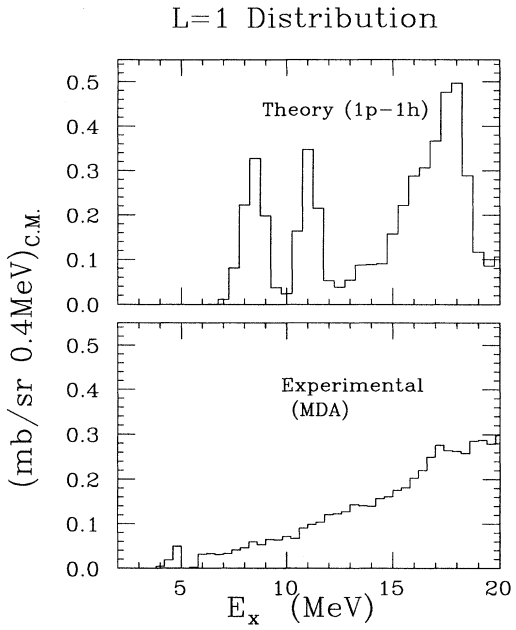

FIG. 13. Dipole and spin-dipole differential cross section (bottom half) obtained at 10° from the MDA is compared with predicted DWIA cross section (top half) obtained using OBDME from the OXBASH calculation (see text).

spectrum, after appropriate normalization. This normalization is chosen such that an $L = 1$ angular distribution has equal yields at both angles. The subtracted spectrum should contain mainly transitions characterized with $L = 0$, assuming that higher multipoles have a similar ratio of yields at these two angles or that they have a small yield at 0°. We obtained a resulting spectrum very similar to the $L = 0$ spectrum obtained in the MDA with a sum $L = 0$ cross section up to 20 MeV differing only by a few percent from the values obtained in the MDA.

We present in Fig. 12, values for polarization observables estimated in the 0° spectrum for the ^{10}B(p,n)^{10}C reaction. The data have been binned in 2 MeV bins size. In particular, we note that the energy distribution of D_{NN} values up to about 25 MeV excitation has negative values. This seems to indicate a preponderance of spin flip transitions and in particular unnatural parity transitions [32].

E. Dipole strength

No known negative parity states are reported for ^{10}C [23]. However in the mirror nuclei ^{10}Be, negative parity states are reported above 6 MeV of excitation. In the MDA (Fig. 10) $\Delta L = 1$ transitions are noted above 5 MeV of excitation. The obtained $\Delta L = 1$ differential cross section at $\theta_{\rm lab} = 10°$ is presented in the bottom half of Fig. 13.

Two neutron groups at about 17.2 and 20.2 MeV excitation in ^{10}C appear in the $L = 1$ spectrum obtained in the MDA. See bottom half of Fig. 10. As indicated above these are probably 2^- or 1^- resonances that have also been observed as $T = 1$ in ^{10}B [23]. We have used the code OXBASH to obtain OBDME for 1p-1h ($p \rightarrow sd$ transitions) negative transitions that extend up to about 21 MeV excitation energy in ^{10}C. The DWIA cross section calculations for all these states at $\theta_{\rm lab} = 10°$ is presented in Fig. 13 (top half) where it is compared with the MDA results (bottom half). The DWIA dipole and spin-dipole cross sections at the calculated eigenvalue excitation energies are shown as a sum of Gaussian distributions with 1 MeV FWHM to match the energy resolution of the experimental data. It is clear from the figure that the simple 1p-1h calculations show a very different concentration of the observed dipole and spin-dipole strength. It is likely that a shell model calculation in a larger model space would reproduce the data better. We have estimated from the $L = 1$ MDA results and the DWIA calculated cross section that only about 72% of the predicted 1p-1h strength has been observed up to 15 MeV of excitation. However, the calculated 1p-1h dipole and spin-dipole strength extends only up to about 21 MeV of excitation, while the MDA seems to indicate that the empirical strength extends to higher excitation energies (see Fig. 10) as was the case for the GT strength.

It is well known that, at intermediate energies close to 200 MeV, the charge exchange (p,n) reaction excites preferentially spin-transfer transitions. Thus, it is very likely that the transitions observed here are $\Delta J = 2^-$ transitions. However, the ^{10}B has a J^π(g.s.) $= 3^+$ which implies that either states with 1^- or 2^- or higher negative J values may be excited in the present study.

V. CONCLUSIONS

We have measured the ^{10}B(p,n)^{10}C reaction at $E_p = 186$ MeV to study the $M3$ stretched ground-state tran-

sition, to study the GT and spin dipole energy distribution and to obtain structure information to final states in ^{10}C. Results for the $M3$ stretched ground-state transition agree well with cross section calculations and polarization observables. The distribution of GT strength seems to be extended to a much higher energy than the predicted results of 1p-1h calculations. A similar observation may be made for the spin dipole strength. Resonances at 16.5, 17.3 and 20.3 MeV excitation energy in ^{10}C seem to be the analogs of 2^+, 2^-, and 1^- states previously observed in ^{10}B.

ACKNOWLEDGMENTS

The authors would like to thank Bill Lozowski for the careful target preparations and acknowledge the helpful and informative discussions with John Millener. This work was supported in part by the NSF.

[1] R.S. Hicks *et al.*, Phys. Rev. Lett. **60**, 905 (1988).
[2] S. Cohen and D. Kurath, Nucl. Phys. **73**, 1 (1965); T.-S.L. Lee and D. Kurath, Phys. Rev. C **21**, 293 (1980).
[3] P.R. Lewis *et al.*, Nucl. Phys. **A532**, 583 (1991).
[4] H. Baghaei, R.A. Lindgren, P. Slocum, E.J. Stephenson, A.D. Bacher, S. Chang, J. Lisantti, J. Liu, C. Olmer, S. Wells, S.W. Wissink, B.L. Clausen, J.A. Carr, S.K. Yoon, and F. Petrovich, Phys. Rev. Lett. **69**, 2054 (1992).
[5] N. Mangelson, F. Ajzenberg-Selove, M. Reed, and C.C. Lu, Nucl. Phys. **88**, 137 (1966).
[6] M.J. Schneider, B.W. Ridley, M.E. Rickey, J.J. Kraushaar, and W.R. Zimmerman, Phys. Rev. C **12**, 335 (1975).
[7] N. Willis, I. Brissaud, L. Bimbot, Y. Le Bornec, and B. Tatischeff, Nucl. Phys. **A261**, 45 (1976).
[8] D. Bachelier, M. Bernas, I. Brissaud, P. Radvanyi, and M. Roy, Phys. Lett. **16**, 304 (1965).
[9] J.R. Shepard, R.E. Anderson, J.J. Kraushaar, and R.A. Ristinen, Nucl. Phys. **A322**, 92 (1979).
[10] S. Dahlgren P. Grafström, B. Höistad, and A. Åsberg, Nucl. Phys. **A204**, 53 (1973).
[11] G.J. Lolos, E.L. Mathie, P.L. Walden, B. Jones, E.G. Auld, and R.B. Taylor, Phys. Rev. C **25**, 1082 (1982).
[12] C.D. Goodman, J. Rapaport, D.E. Bainum, and C.E. Brient, Nucl. Instrum. Methods **151**, 125 (1978).
[13] T.N. Taddeucci, C.D. Goodman, R.C. Byrd, T.A. Carey, D.J. Horen, J. Rapaport, and E. Sugarbaker, Nucl. Instrum. Methods **A241**, 448 (1985).
[14] T.N. Taddeucci, W.P. Alford, M. Barlett, R.C. Byrd, T.A. Carey, D.E. Ciskowski, C.C. Foster, C. Gaarde, C.D. Goodman, C.A. Goulding, E. Gülmez, W. Huang, D.J. Horen, J. Larsen, D. Marchlenski, J.B. McClelland, D. Prout, J. Rapaport, L.J. Rybarcyk, and W.C. Sailor, Phys. Rev. C **41**, 2548 (1990).
[15] J. Rapaport, C.C. Foster, C.D. Goodman, C.A. Goulding, T.N. Taddeucci, D.J. Horen, E.R. Sugarbaker, C. Gaarde, J. Larsen, J.A. Carr, F. Petrovich, and M.J. Threapleton, Phys. Rev. C **41**, 1920 (1990).
[16] M.A. Moinester, Can. J. Phys. **65**, 660 (1987).
[17] R. Schaeffer and J. Raynal, Program DWBA70 (unpublished); extended version DW81 by J.R. Comfort (unpublished).
[18] J.R. Comfort and B.C. Karp Phys. Rev. C **21**, 2162 (1980).
[19] M.A. Franey and W.G. Love, Phys. Rev. C **31**, 488 (1985).
[20] F.P. Brady, T.D. Ford, G.A. Needham, J.L. Romero, D.S. Sorenson, C.M. Castaneda, J.L. Drummond, E.L. Hjort, B. McEachern, N.S.P. King, and D.J. Millener, Phys. Rev. C **43**, 2284 (1991).
[21] B.A. Brown *et al.*, The Oxford-Buenos Aires-MSU shell-model code OXBASH, Michigan State University Cyclotron Laboratory Report 524, 1986.
[22] D.J. Millener and D. Kurath, Nucl. Phys. **A255**, 315 (1975).
[23] F. Ajzenberg-Selove, Nucl. Phys. **A490**, 1 (1988).
[24] T. Massey, Ohio University, private communication.
[25] W.G. Love *et al.*, Can. J. Phys. **65**, 536 (1987); W.G. Love, M.A. Franey and F. Petrovich, in *Spin Excitations in Nuclei*, edited by F. Petrovich *et al.* (Plenum, New York, 1984), p. 205.
[26] C.D. Goodman, R.C. Byrd, I.J. Van Heerden, T.A. Carey, D.J. Horen, J.S. Larsen, C. Gaarde, J. Rapaport, T.P. Welch, E. Sugarbaker, and T.N. Taddeucci, Phys. Rev. Lett. **54**, 877 (1985).
[27] J. Rapaport, D. Wang, J.A. Carr, F. Petrovich, C.C. Foster, C.D. Goodman, C. Gaarde, J. Larsen, C.A. Goulding, T.N. Taddeucci, D. Horen, and E. Sugarbaker, Phys. Rev. C **36**, 500 (1987).
[28] B.K. Park, J. Rapaport, J.L. Ullmann, A.G. Ling, D.S. Sorenson, F.P. Brady, J.L. Romero, C.R. Howell, W. Tornow, and C.T. Rönnqvist, Phys. Rev. C **45**, 1791 (1992).
[29] A. Celler, W.P. Alford, R. Abegg, D. Frekers, O. Häusser, R. Helmer, R.S. Herderson, K.P. Jackson, R. Jeppesen, B. Larson, J. Mildenberger, B.W. Pointon, A. Trudel, M. Vetterli, and S. Yen, Phys. Rev. C **43**, 639 (1991).
[30] T.N. Taddeucci, R.C. Byrd, T.A. Carey, D.E. Ciskowski, C.C. Foster, C. Gaarde, C.D. Goodman, E.Gülmez, W. Huang, D.J. Horen, J. Larsen, D.Marchlenski, J.B. McClelland, D. Prout, J. Rapaport, L.J. Rybarcyk, E. Sugarbaker, I.J. Van Heerden, and C.A. Whitten, Jr., Phys. Rev. C **42**, 935 (1990).
[31] C.D. Goodman and S.D. Bloom, in *Spin Excitations in Nuclei* [25], p. 143.
[32] J.M. Moss, Phys. Rev. C **26** 727 (1982); J.M. Moss, in *Spin Excitations in Nuclei* [25], p. 355.